How to cite: *Angew. Chem. Int. Ed.* **2025**, e19602
doi.org/10.1002/anie.202519602

3D Printing

Open-Air, Ultrafast Photoiniferter Polymerization Enables 3D Printing with Low-Viscosity Resins

Zipeng Zhang, Dong Su, Mingzhou Zhang, Zesheng An, Cyrille Boyer,* and Chenyu Wu**

Abstract: Photo-curing 3D printing is fundamentally challenged by the formation of heterogeneous networks with uneven cross-linking densities and unreacted monomer residues, which compromise the integrity and performance of printed parts. While photo-controlled radical polymerization (photo-RDRP) offers a path to precise network control, it is often limited by sluggish kinetics, necessitating viscous resins to compensate for slow curing rates. To overcome this, we employed a computer-guided strategy to design a new photoiniferter, dithioindazolylcarboxylate (DTI). Computational analyses predicted DTI would be an efficient and oxygen-tolerant photoiniferter. Under 415 nm light (10 mW cm^{-2}), DTI enabled the photoiniferter polymerization of methyl acrylate with an apparent propagation rate (k_p^{app}) of 0.809 min^{-1}, over four-fold higher than that of the existing dithiopyrazolylcarboxylate (DTP) with a k_p^{app} of 0.196 min^{-1} in equivalent conditions under 425 nm (optimum for k_p^{app}). This was achieved while maintaining low molecular weight dispersity ($Đ < 1.1$). DTI also exhibited better oxygen tolerance, maintaining 65.9% of its k_p^{app} (with respect to that under nitrogen) under an air-purging condition (1 mL 30 s^{-1}), as compared to 13.3% for DTP under the same condition. This enabled ultrafast digital light processing (DLP) 3D printing at just 8 s per layer using routine low-viscosity acrylic resins, producing high-resolution, complex centimeter-scale prototypes. The technology also enabled photo-curing of anticorrosion coatings with an adhesion strength of 13.53 MPa and 720 h resistance to acetic acid salt spray.

Introduction

Additive manufacturing technologies have seen a surge in recent years, enabling rapid prototyping of complex geometries.[1] Among these, photo-curing 3D printing stands out for its layer precision and rapid curing capabilities.[2–4] However, conventional methods rely on photo-initiated free-radical polymerization,[5] yielding heterogeneous networks with uneven cross-linking densities, topological defects, and residual monomers.[6,7] Visible-light-controlled reversible deactivation radical polymerization (photo-RDRP)[8–16] addresses these limitations by leveraging reversible radical termination and degenerative chain transfer mechanisms.[17–27] This approach produces well-defined polymer networks with homogeneous chain lengths[28–32] and tailorable mechanical properties.[33] Critically, the high end-group fidelity inherent to photo-RDRP allows for advanced functionalities, including self-healing,[32] post-printing "welding",[34,35] and surface post-functionalization,[36] thereby expanding the capabilities of 3D-printed materials.

Despite these advantages, the industrial integration of photo-RDRP with photo-curing 3D printing is restricted by sluggish polymerization kinetics.[28] To compensate for these slow kinetics, polymer chemists have used viscous acrylate or acrylamide macromonomers for complex object fabrication,[8,28,33,34,37–40] a compromise that hinders the practical adoption of the technology (detailed in Section S4).[41–43]

The kinetic sluggishness of catalyzed photo-RDRP arises from short-lived transient encounter complexes between the photocatalyst and initiator during dissociative electron transfer.[44] A "permanent encounter complex", which forms a covalent bond between the photocatalyst and initiator, represents a kinetic optimum by eliminating these transient steps. Photoiniferter polymerization[45–47] embodies this concept by integrating photoinitiator, chain transfer agent, and terminator roles into a single molecule, theoretically offering superior kinetics (see Section S5.1). However, conventional photoiniferter systems have failed to translate this mechanistic promise into rapid, industrially viable polymerization kinetics.[48]

Recent advances in photoiniferter polymerization have revitalized this technique.[45,46] For example, xanthates[34,49–54] exhibit faster kinetics than trithiocarbonates,[55–67] dithiobenzoates,[68–70] and dithiocarbamates,[71–73] but with poor polymerization control, resulting in high

[*] Z. Zhang, M. Zhang, Prof. C. Wu
Qingdao Institute for Theoretical and Computational Science, Center for Optics Research and Engineering, Shandong University, Qingdao 266237, China
E-mail: w@sdu.edu.cn

D. Su, Prof. C. Boyer
Cluster for Advanced Macromolecular Design, School of Chemical Engineering, Faculty of Engineering, University of New South Wales, Sydney NSW 2033, Australia
E-mail: cboyer@unsw.edu.au

Prof. Z. An
State Key Laboratory of Supramolecular Structure and Materials, College of Chemistry, Jilin University, Changchun 130012, China
E-mail: anzesheng@jlu.edu.cn

Additional supporting information can be found online in the Supporting Information section

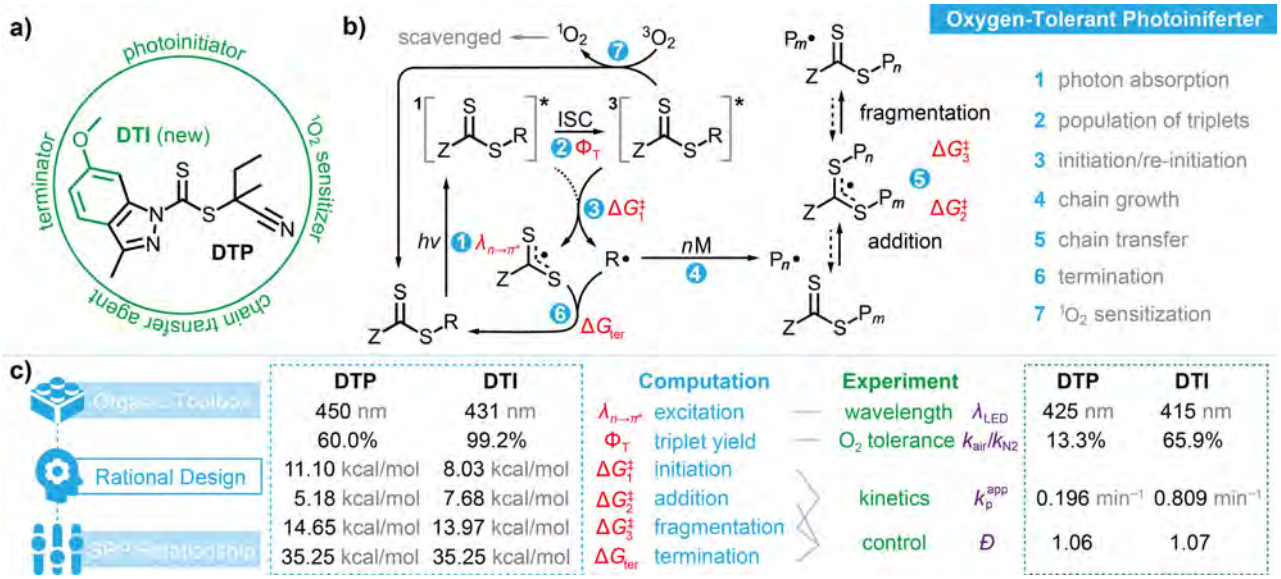

Scheme 1. Chemical structure, mechanism, and design of oxygen-tolerant photoiniferter. a) Chemical structure of DTI (6-methoxy-3-methyl-1H-indazole-1-carbodithioic acid 1-cyano-1-methylpropyl ester) highlighting its multifunctional roles (photoinitiation, chain transfer, termination, and photosensitization). The existing photoiniferter DTP (3,5-dimethyl-1H-pyrazole-1-carbodithioic acid 1-cyano-1-methylpropyl ester) as a reference structure is the black part. b) The oxygen-tolerant photoiniferter mechanism featuring photon absorption (wavelength $\lambda_{n\to\pi^*}$), triplet population (quantum yield Φ_T), photolysis (barrier $\Delta G_1^\ddagger$), addition (barrier $\Delta G_2^\ddagger$), and fragmentation (barrier $\Delta G_3^\ddagger$) in chain transfer, as well as termination (change ΔG_{ter}). c) Computer-guided design workflow for DTI integrating computational prediction with experimental validation, with more details in Section S5.5. **Notes**: The photoiniferter in this work adopts a thiocarbonylthio (Z—C(=S)—S—R) structure, where Z is the function group and R is the initiating group. M is monomer, ahead of which *n* is the number of monomers. P_n and P_m are polymers with *n* and *m* degrees of polymerization, respectively. ΔG is Gibbs free energy change and $\Delta G\ddagger$ is the Gibbs free energy barrier. ISC is intersystem crossing. BDE is bond dissociation energy. General computational method[78]: ωB97X[79]-D3[80]/def2-SVP[81] with SMD-DMSO[82] solvation model. SPP is structure–property–performance. λ_{LED} is the nominal wavelength of the light emitting diode (LED). k_p^{app} is the apparent propagation rate. The ratio k_{air}/k_{N_2} represents the oxygen tolerance, defined as the fraction of k_p^{app} retained under 1 mL/ 30 s^{-1} air-purging (k_{air}) relative to the value under nitrogen (k_{N_2}). $Đ$ is the molecular weight dispersity.

molecular weight dispersity ($Đ > 1.3$) for acrylates and acrylamides.[34,49,74,75] While pyrazole-based photoiniferters, i.e., dithiopyrazolylcarboxylate (DTP),[75,76] improved polymerization control ($Đ < 1.1$ for acrylates and acrylamides) with fast kinetics comparable to xanthates, their polymerization kinetics and oxygen tolerance remained insufficient for demanding applications, such as 3D printing.

Here, we bridge this gap through a computer-guided strategy leveraging structure–property–performance relationships[12,77] to design a multifunctional photoiniferter, dithioindazolylcarboxylate (DTI, Scheme 1a and b). Quantum chemical calculations predicted DTI would exhibit enhanced kinetics, control, and oxygen tolerance, compared to the existing system DTP, a prediction we validated experimentally (Scheme 1c). In the photoiniferter polymerization of methyl acrylate (MA), DTI achieved an apparent propagation rate ($k_p^{app} = 0.809\,min^{-1}$), which is over four-fold higher than that of the previous benchmark DTP ($k_p^{app} = 0.196\,min^{-1}$) under equivalent conditions, while maintaining excellent polymerization control ($Đ < 1.1$). Furthermore, DTI displayed enhanced oxygen tolerance, retaining 65.9% of its k_p^{app} under air-purging at 1 mL 30 s^{-1}, compared to only 13.3% for DTP. This performance enabled 8 s/layer photo-curing 3D printing of complex centimeter-scale prototypes using various low-viscosity acrylic resins.

Results and Discussion

Computer-Guided Design

The performance of photo-RDRP is dictated by its polymerization kinetics, polymerization control, and oxygen tolerance.[12] In photoiniferter polymerization (Scheme 1), kinetics are governed by the photolysis energy barrier $\Delta G_1^\ddagger$ and the fragmentation barrier $\Delta G_3^\ddagger$, which promotes efficient radical release and reduce radical trapping time, respectively. Polymerization control is influenced by the addition barrier $\Delta G_2^\ddagger$ for chain transfer intermediate formation (a lower value increases chain transfer likelihood) through controlling the chain transfer constant (Section S5.2.2), and the termination energy change ΔG_{ter} (a more negative value favors reversible deactivation). Crucially, oxygen tolerance relies on high triplet quantum yield (Φ_T) enabling photosensitized generation of singlet oxygen ($^1O_2$) via energy transfer from the triplet-state photoiniferter to ground-state oxygen ($^3O_2$), followed by $^1O_2$ scavenging.[12]

Guided by these structure–property–performance relationships[12,77] (Section S5.2), we rationally designed a new photoiniferter, DTI, characteristic of a methoxy-substituted benzene ring fused to the pyrazole ring as the Z group, strategically engineered to synergistically enhance

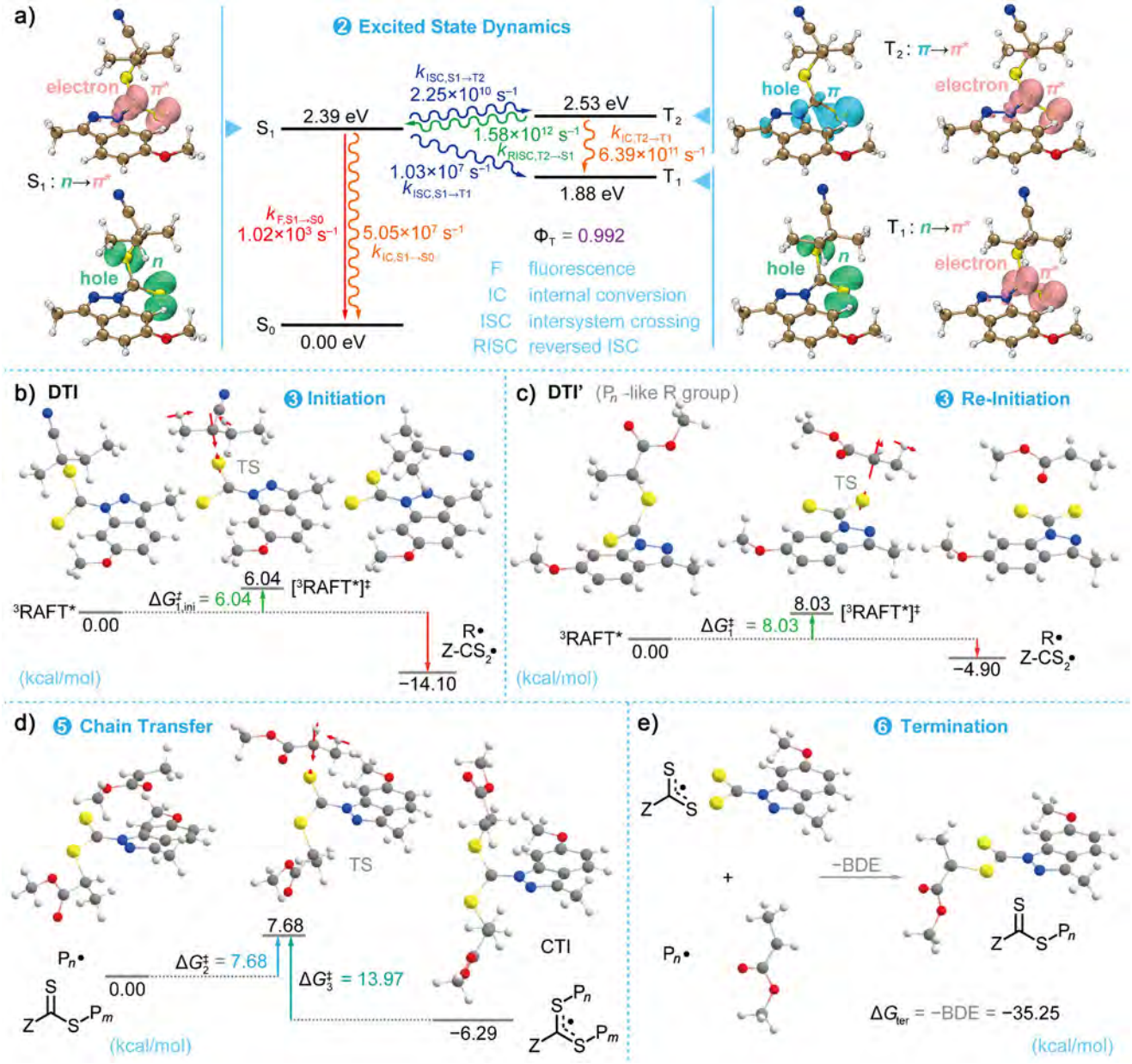

Figure 1. Theoretical analysis on oxygen-tolerant photoiniferter polymerization. a) Jablonski diagram for excited state dynamics to derive the triplet quantum yield (Φ_T), with electron-hole analysis for S_1, T_2, and T_1. b–e) Thermodynamic studies of photolysis of DTI (b) and DTI' (c) along with chain transfer (d) and termination (e). **Note**: a) k_{ISC} are rate constants for intersystem crossing (ISC) of the $S_1 \rightarrow T_2$ and $S_1 \rightarrow T_1$ transitions, whereas k_{RISC} are the rate constants for reverse transitions $T_2 \rightarrow S_1$ and $T_1 \rightarrow S_1$ ($8.12 \times 10^5\ s^{-1}$). k_{IC} are rate constants for internal conversion (IC) of the $S_1 \rightarrow S_0$ and $T_2 \rightarrow T_1$ transitions. k_F is the fluorescence rate constant. These rate constants derive quantum yield for T_1 to be $\Phi_T = 99.2\%$ (detailed in Section S13.3). b) DTI' adopts a propanoic acid methyl ester as the R group, which represents P_n in chain growth. e) BDE is the bond dissociation energy. General computational method[78]: ωB97X[79]-D3[80]/def2-SVP[81]/SMD-DMSO,[82] temperature assumed as 298 K. Multiwfn[83] was used to conduct electron-hole analysis with VMD[84] for visualization.

all performance metrics (Section S5.3). As predicted by computational analysis (Section S5.4), DTI exhibits low energy barriers for photolysis ($\Delta G_1^{\ddagger} = 8.03\,kmol^{-1}$, Figure 1c) and fragmentation ($\Delta G_3^{\ddagger} = 13.97\,kmol^{-1}$, Figure 1d) using MA as the example monomer. These results predict faster kinetics in comparison with the state-of-the-art system DTP (Section S5.4.7). Additionally, its low addition barrier ($\Delta G_2^{\ddagger} = 7.68\,kmol^{-1}$, Figure 1d) and highly negative termination energy change ($\Delta G_{ter} = -35.25\,kmol^{-1}$, Figure 1e) ensures precise polymerization control. Encouragingly, DTI is predicted with a high Φ_T (99.2%, Figure 1a), facilitating fast photolysis via longer-lived triplet states, and establishing the mechanistic foundation for $^1O_2$ photosensitization, a pathway to oxygen tolerance (Section S5.2.3). These computational results predict that DTI significantly outperforms the state-of-the-art photoiniferter,[75] DTP (higher $\Delta G_1^{\ddagger}$ and higher $\Delta G_3^{\ddagger} = 14.65\,kmol^{-1}$ for slower kinetics than DTI, comparable but lower $\Delta G_2^{\ddagger} = 5.18\,kmol^{-1}$ for similar

polymerization control to DTI, and substantially lower Φ_T signalling compromised oxygen tolerance according to Section S5.4.7). The predicted better photoiniferter performance of DTI over this existing system was confirmed experimentally (Section S5.5.3 and *vide infra*). Furthermore, the characteristic $n \rightarrow \pi^*$ excitation wavelength $\lambda_{n\rightarrow\pi^*}$ is computed at 431 nm (Section S5.4.1), aligning closely with the 405 nm commercial LED standard in photo-curing 3D printers, ensuring direct compatibility. Collectively, this computational analysis validates DTI as a potent, high-performance, and oxygen-tolerant photoiniferter.

Synthesis and Experimental Validation

The DTI was then synthesized through a two-step reaction from low-cost commercial chemicals (see Section S1). Its structure was confirmed by ^{1}H nuclear magnetic resonance (NMR) spectroscopy, ^{1}H-^{13}C heteronuclear single quantum coherence (HSQC) NMR spectroscopy, and high-resolution mass spectrometry (see Section S3.1). Photolysis kinetics under 425 nm light (10 mW cm^{-2}) in dimethyl sulfoxide (DMSO) with 2,2,6,6-tetramethylpiperidinyl-1-oxide (TEMPO) as the radical scavenger (see Section S5.5.1) revealed ultrafast photodissociation for DTI (4.38×10^{-1} s^{-1}, Figure S13A, blue line). To evaluate the reinitiating ability of DTI after MA addition, we synthesized DTI' (Figure S13D), a structural analogue bearing a propanoic acid methyl ester as the R group. This derivative exhibited rapid photolysis (6.72×10^{-2} s^{-1}, Figure S13A, green line), confirming its reinitiating ability. On the other hand, the photosensitization ability was evaluated using DTI-Hex (*n*-hexane R-group analogue, Figure S13D) to minimize interference from carbon-centered radicals (R$^\bullet$). $^1O_2$ generation kinetics monitored by 9,10-dimethylanthracene (DMAn) and 2,2,6,6-tetramethylpeperidine (TEMP) trapping demonstrated comparable photosensitization capability to Eosin Y[12,85] (Section S5.5.2).

Kinetic Studies and Polymerization Tests

A 415 nm 10 mW/cm^2 light emitting diode (LED) was used for kinetic studies on photoiniferter polymerization of MA ([MA]:[DTI] = 200:1, MA:DMSO = 1:1 *v*/*v*, 25°C), as it provided the maximum k_p^{app} based on an evaluation of wavelength-dependent photochemical efficiencies[86–88] (Section S6.2). Under nitrogen, the system achieved a k_p^{app} of 0.809 min^{-1} (Figure 2a, blue line), which is more than four-fold faster than DTP (Section S5.5.3). Despite this high rate, the polymerization maintained excellent control, with a linear evolution of number-average molecular weights (M_n) that closely matched theoretical values (Figure 2b, blue points) and a dispersity as low as $Đ$ <1.1 (Figure 2c, blue points). Most encouragingly, the new photoiniferter achieved superior oxygen tolerance in polymerization, as anticipated by the computational and experimental analyses (Sections S5.4.2 and S5.5.2). As shown in Figure 2, polymerization in air-present conditions retained 81.2% of the k_p^{app} (0.657 min^{-1}), while open-air conditions retained 71.4% (0.578 min^{-1}), both without sacrificing polymerization control. Even under a harsh air-purged condition (1 mL 30 s^{-1}), the system retained 65.9% of the k_p^{app} (0.533 min^{-1}) with very limited compromise in control. In all cases, we observed narrow molecular weight distributions with clear shift, short induction periods (∼ 1 min), and excellent temporal control, conclusively validating the robustness and oxygen tolerance of the DTI-mediated approach. More detailed data are recorded in Section S5.5.3. The observed induction periods show no significant differences with varied oxygen content (0.87 min for nitrogen, 0.88 min for air-present, 0.91 min for open-air, and 0.86 for air-purging atmospheres; Table S1), indicating a negligible influence on induction periods from oxygen. This is consistent with observations in ZnTPP-catalyzed PET–RAFT polymerization.[89] The specific oxygen-tolerance mechanism common to both systems will be explored in future work. The minor variations in the induction period (∼0.05 min) are within experimental error, likely arising from irradiation timing or incidental light exposure. Instead, the observed ∼0.05 min induction period is attributed to retarded initiation from the R group of DTI, as discussed in Section S5.4.4.

On a comparative basis, the optimal LED irradiation wavelengths (λ_{LED}) for DTI and DTP, corresponding to the highest k_p^{app}, were determined to be 415 and 425 nm, respectively, via a scan using LEDs (full width at half maximum ∼20 nm) with central emission peaks spaced at 10 nm intervals in the visible range (Section S6.2). This renders DTI more favorable for widely used 405 nm commercial LEDs in photo-curing technologies, retaining 83.5% of its k_p^{app} at 405 nm relative to 415 nm, whereas DTP retains only 64.6% at 405 nm relative to 425 nm. In terms of kinetic efficiency, DTI achieved a $k_p^{app} = 0.809$ min^{-1} ($\lambda_{LED} = 415$ nm), which is over four-fold higher than that of DTP ($k_p^{app} = 0.196$ min^{-1}, $\lambda_{LED} = 425$ nm) under equivalent conditions (Section S6.2). The $Đ$ reached for DTI and DTP were both below 1.1, indicating comparable polymerization control. Importantly, under air-purging at 1 mL 30 s^{-1}, DTI exhibited better oxygen tolerance with a k_{air}/k_{N_2} ratio of 65.9% (where k_{air} and k_{N_2} denote k_p^{app} under 1 mL 30 s^{-1} air-purging and nitrogen atmospheres, respectively), significantly higher than the 13.3% ratio observed for DTP under identical conditions.

^{1}H NMR analysis of purified polymers revealed the characteristic signal of the methoxy protons (δ 3.80–3.85 ppm) of DTI. This signal was used to calculate the experimental degree of polymerization (DP_n), which closely matched the theoretical values. This consistency was observed under both nitrogen and air-present conditions, indicating that polymerization control and end-group integrity were maintained even in the presence of oxygen (Section S7.2). To further validate the living nature of the DTI system, chain extension experiments were successfully performed. A low-molecular-weight polyDMAm (M_n = 4,000 g mol^{-1}, $Đ$ = 1.06) and polyMA (M_n = 4,700 g mol^{-1}, $Đ$ = 1.06) were successfully chain-extended into higher-molecular-weight block copolymers (polyDMAm-*b*-polyMA, M_n = 41,700 g mol^{-1}, $Đ$ = 1.17, and polyMA-*b*-polyDMAm, M_n = 40,800 g mol^{-1}, $Đ$ = 1.14). The absence of a low-molecular-weight tail in the final products confirms the high end-group fidelity and

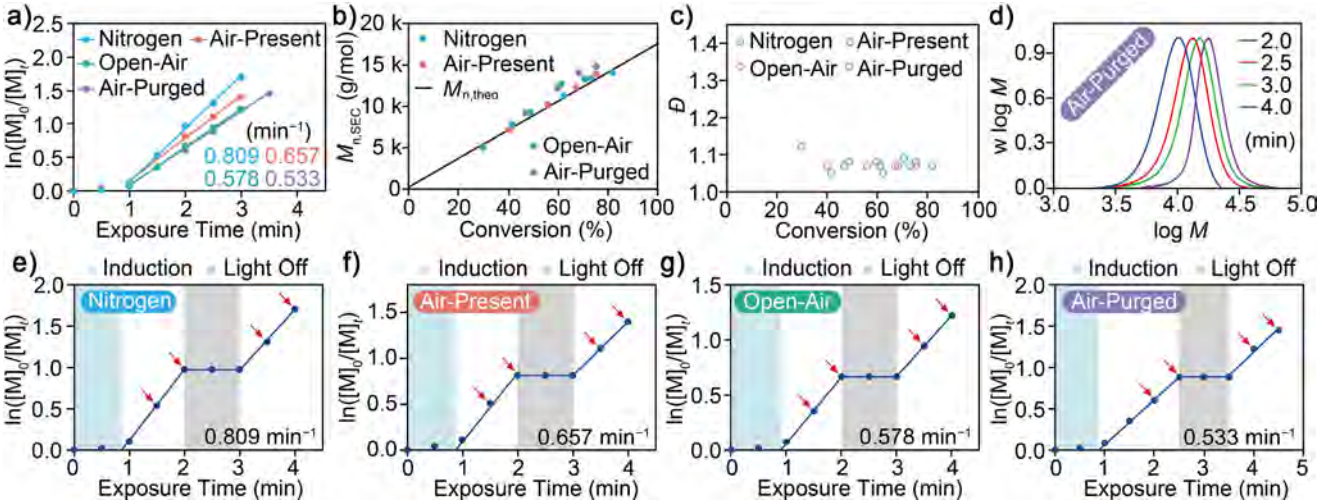

Figure 2. Oxygen-tolerant photoiniferter polymerization kinetics. a) Plots of $\ln([M]_0/[M]_t)$ versus light exposure time with k_p^{app} in nitrogen (blue), air-present (red), open-air (green), and 1 mL 30 s^{-1} air-purging (purple) atmospheres. b and c) Plots of M_n b) and $Đ$ c) versus monomer conversion in corresponding atmospheres. d) Plot of normalized molecular weight distributions of polyMA sampled at different time points (red arrows in H) in the 1 mL 30 s^{-1} air-purging polymerization. e–h) Plots of $\ln([M]_0/[M]_t)$ versus time demonstrating temporal control of the nitrogen e), air-present f), open-air g), and air-purged h) systems. The air-purged system is injected with 1 mL air every 30 s using a syringe with a thin needle into the 0.4 mL polymerization solution.

Table 1: High-molecular-weight photoiniferter polymerization.[a)]

Monomer	[M]: [DTI][b)]	Solvent	Time[c)] (min)	α[d)]	$M_{n,\,theo}$[e)] (g mol^{-1})	$M_{n,\,SEC}$[f)] (g mol^{-1})	$Đ$[g)]
MA	400:1	DMSO	4	85.1%	29 600	33 800	1.10
MA	1000:1	DMSO	5	86.5%	74 800	79 900	1.11
MA	10000:1	DMSO	10	71.0%	611 700	716 700	1.57
MA	10000:1	DMSO	10	70.7%	609 100	759 900	1.50
MA	20000:1	DMSO	20	71.3%	1 227 700	1 636 000	1.41

[a)] MA polymerizations targeting different degrees of polymerization using DTI were conducted under 10 mW cm^{-2} 415 nm light under nitrogen. All reactions were performed at room temperature, MA:DMSO = 1:1 *v*/*v*. [b)] Molar ratios between the monomer and the photoiniferter (DTI). [c)] Irradiation time of the reaction solution. [d)] Monomer conversion determined by Fourier-transform near-infrared (FT-NIR) spectroscopy. [e)] Theoretical value of the number-averaged molecular weight (M_n) calculated based on α. [f)] Absolute M_n obtained by size exclusion chromatography coupled with multi-angle light scattering (SEC-MALS). [g)] Molecular weight dispersity determined by SEC-MALS; the $Đ$ values determined do not possess the accuracy of two decimal places, but the second digit is provided for reference.

successful chain extension (see Section S10). These results provide compelling evidence that DTI produces negligible amounts of "dead chain" polymers. The resulting polymer chains effectively retain their active RAFT end groups, which is a prerequisite for the subsequent synthesis of well-defined block copolymers. Furthermore, we demonstrated the ability to synthesize polymers with high molecular weights up to > 1 000 000 g mol^{-1}albeit with a sacrifice in control with $Đ$ around 1.5 determined by size exclusion chromatography coupled with multi-angle light scattering (SEC-MALS; Table 1).

To evaluate solvent and monomer compatibility, a broad range of solvents and monomers were tested (Table 2). All solvents, including polar protic (MeOH), polar aprotic (DMSO, DMF, MeCN, Acetone, EtOAc, THF, and DCM), and non-polar (cyclohexane), facilitated controlled polymerization ($Đ$ < 1.2) with rapid kinetics (Table 2). Analyses of different monomers were also shown in Table 2. MAMs, including acrylates (MA, EA, *t*-BA, BzA, and PA) and acrylamides (DMAm, NAM, and NIPAm), resulted in good polymerization control ($Đ$ < 1.2 or $Đ$ ~ 1.2), whereas methyl methacrylate (MMA) and styrene (St) lost control ($Đ$ > 3.5). LAMs, including *N*-vinylpyrrolidone (NVP) and vinyl pivalate (VP), yielded some polymerization control with $Đ$ between 1.3 and 1.4. However, for vinyl acetate (VA), the dispersity ($Đ$) was observed to be approximately 1.6, indicating less control. Solvents with higher polarity (e.g., DMSO with the highest polarity index[90] of 7.2) generally promote faster kinetics (Table 2), likely by stabilizing the polarized transition state during photoiniferter activation.[89,91] Nevertheless, the polarity cannot fully explain the trend in Table 2, such as the slower kinetics in highly polar MeCN or faster kinetics in protic MeOH, which might include potential electronic transitions, hydrogen bonding, or acid-enhanced[65] effects. This aspect needs further investigation beyond the scope of this work. Similarly, monomer polarity also influences polymerization kinetics; however, monomer reactivity governed by electronic and steric effects around the vinyl group complicates the overall monomer effect. This aspect will be evaluated in future work.

Digital Light Processing 3D Printing

The enhanced kinetics and oxygen tolerance of DTI-mediated photoiniferter polymerization over the existing DTP system, encouraged us to apply it to digital light processing (DLP) 3D printing, a technology typically requires fast photocuring rates. Using a commercial 405 nm DLP 3D printer

Table 2: Solvents and monomers tested for DTI-mediated photoiniferter polymerization.[a)]

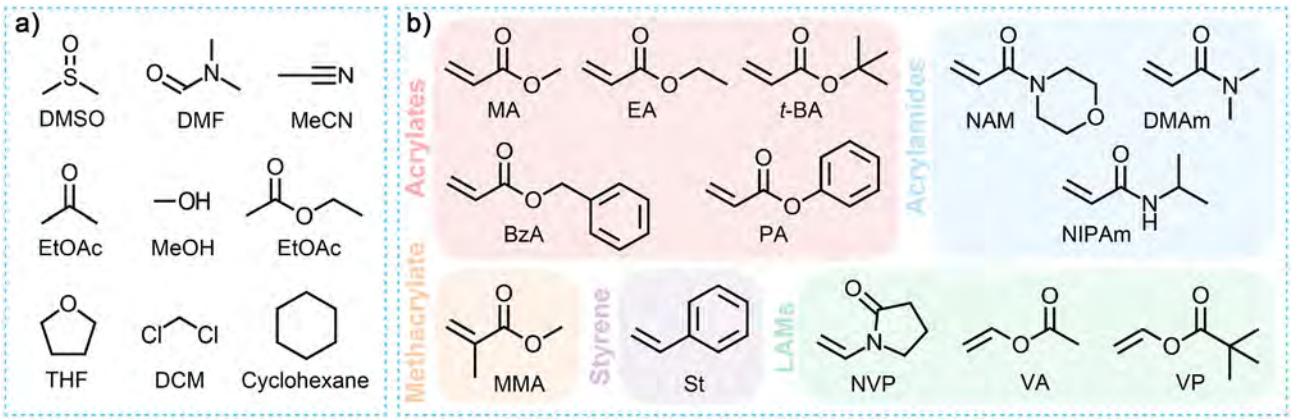

Monomer	Solvent	P'[b)]	Time[c)] (min)	α[d)]	$M_{n,\,theo}$[e)] (g mol^{-1})	$M_{n,\,SEC}$[f)] (g mol^{-1})	$Đ$[g)]
MA	DMSO	7.2	3	79.1%	13 900	13 800	1.08
MA	DMF	6.4	3	58.0%	10 300	10 800	1.13
MA	MeCN	5.8	3	35.4%	6400	7600	1.12
MA	Acetone	5.1	3	46.0%	8200	8600	1.13
MA	MeOH	5.1	3	59.0%	10 500	9900	1.12
MA	EtOAc	4.4	3	21.7%	4100	4600	1.11
MA	THF	4.0	3	49.4%	8800	9000	1.19
MA	DCM	3.1	3	38.6	7 000	7600	1.15
MA	Cyclohexane	0.2	3	29.6	5 400	6800	1.17
NAM	DMSO	3.90	2	81.3	23 300	14 700	1.18
DMAm	DMSO	3.90	5	75.0	15200	17 400	1.07
NIPAm	DMSO	3.90	12	73.3	16 900	15 200	1.15
EA	DMSO	3.90	3	73.1	15 000	15 200	1.13
PA	DMSO	3.90	1.25	71.3	21 400	20 600	1.23
t-BA	DMSO	3.90	4	71.5	18 700	10 000	1.18
BzA	DMSO	3.90	2	76.6	25 200	17 200	1.17
MMA	DMSO	3.90	40	38.2	8000	6 300	3.58
St	DMSO	3.90	12	27.4	6 000	2 500	5.12
VA	DMSO	3.90	600	31.2	5 700	13 100	1.63
VP	DMSO	3.90	600	21.0	5 700	6500	1.40
NVP	DMSO	3.90	40	36.0	8300	8400	1.31

[a)] Polymerizations for different monomers were conducted using DTI under 10 mW cm^{-2} 425 nm light in a nitrogen atmosphere. All reactions were performed at room temperature, [monomer]:[solvent] = 1:1 *v*/*v*. A fixed reaction stoichiometry of [monomer]:[DTI] = 200:1 was used. [b)] Polarity index.[14] [c)] Irradiation time. [d)] Monomer conversion. [e)] Theoretical value of the number-averaged molecular weight (M_n) calculated based on α. [f)] Experimental M_n obtained by size exclusion chromatography. [g)] $Đ$ values determined by SEC do not possess the accuracy of two decimal places; however, the second digit is provided for reference. (a–b) Chemical structures for solvents (a) and monomers (b). MeOH: methanol. EtOH: ethanol. DMSO: dimethyl sulfoxide. DMF: *N*, *N*-dimethylformamide. MeCN: acetonitrile. EtOAc: ethyl acetate. THF: tetrahydrofuran. DCM: dichloromethane. MA: methyl acrylate. EA: ethyl acrylate. *t*-BA: *t*-butyl acrylate. BzA: benzyl acrylate. PA: phenyl acrylate. DMAm: *N*, *N*-dimethylacrylamide. NAM: 4-acryloylmorpholine. NIPAm: *N*-isopropylacrylamide. MMA: methyl methacrylate. St: styrene. VA: vinyl acetate. VP: vinyl pivalate. NVP: *N*-vinylpyrrolidone.

(RayShape P200 UHD, 405 nm, 23 mW cm^{-2}), we formulated resins containing a commercial acrylamide monomer (NAM), crosslinker (TMPTA), and DTI at a common formulation ([NAM]:[TMPTA]:[DTI] = 200:10:1), without any additional photoinitiators or additives. The resin achieved a curing time of 8 s/layer in open air, which enabled efficient fabrication (Table 3). The system proved robust, maintaining a curing time of 10 s per layer even when the printer's light intensity was reduced to its lowest setting (13.8 mW cm^{-2}) (Table 3).

We also tested other common acrylates that are less volatile for open-air 3D printing, including BzA, HEA, IBoA, and BA. All of these monomers were successfully printed with optimal curing times ranging from 14 to 20 s per layer. Even when we reduced the DTI loading by more than half, the system remained robust, delivering comparable layer time (Table 3). This highlights the system's efficiency and its ability to function effectively even with a low concentration of the photoiniferter.

Given the robustness of the system across diverse resins and formulations at high speeds (8–20 s/layer) (Table 3), we fabricated sophisticated centimeter-scale prototypes. To circumvent moisture absorption issues observed in NAM resins during long-term storage, we employed a BzA-based resin formulation ([BzA]:[TMPTA]:[DTI] = 200:40:1). This resin exhibited an optimum curing time of 14 s/layer (Table 3). Using this formulation, world landmark replicas (Figure 3a–d) were successfully printed. The dimensional accuracy of a printed test plate was assessed by calculating the root mean

Table 3: Oxygen-tolerant photoiniferter polymerizations tested for digital light processing 3D printing.[a)]

Monomer	Crosslinker	Photoiniferter	Ratio[b)]	Printing Speed[c)] (s/layer)	Intensity[d)] (mW cm^{-2})
NAM	TMPTA	DTI	200:10:1	8	23 (100%)
NAM	TMPTA	DTI'	200:10:1	8	23 (100%)
NAM	TMPTA	DTI	200:10:1	10	13.8 (60%)
BzA	TMPTA	DTI	200:40:1	14	23 (100%)
HEA	TMPTA	DTI	200:10:1	15	23 (100%)
IBoA	TMPTA	DTI	200:10:1	20	23 (100%)
BA	TMPTA	DTI	200:40:1	20	23 (100%)
NAM	TMPTA	DTI	300:15:1	8	23 (100%)
NAM	TMPTA	DTI	400:20:1	9	23 (100%)
NAM	TMPTA	DTI	500:25:1	9	23 (100%)

[a)] Commercial 3D printer Rayshape P200 UHD (light source: 405 nm wavelength, 23 mW cm^{-2} intensity), with 25 μm layer thickness and 32.5 μm pixel size, was employed for all the 3D printings. [b)] Molar ratio of the monomer, photoiniferter, and crosslinker, [M]:[DTI/DTI']:[crosslinker]. [c)] The optimal printing speed tested with the standard testing model shown in Section S11.4. [d)] The highest irradiation intensity of the commercial 3D printer is 23 mW cm^{-2} which is the default, whereas the lowest intensity that can be set is 13.8 mW cm^{-2} which is 60% of the default. NAM: 4-acryloylmorpholine. TMPTA: trimethylolpropane triacrylate. BzA: benzyl acrylate. HEA: 2-hydroxyethyl acrylate. IBoA: isobornyl acrylate. BA: butyl acrylate.

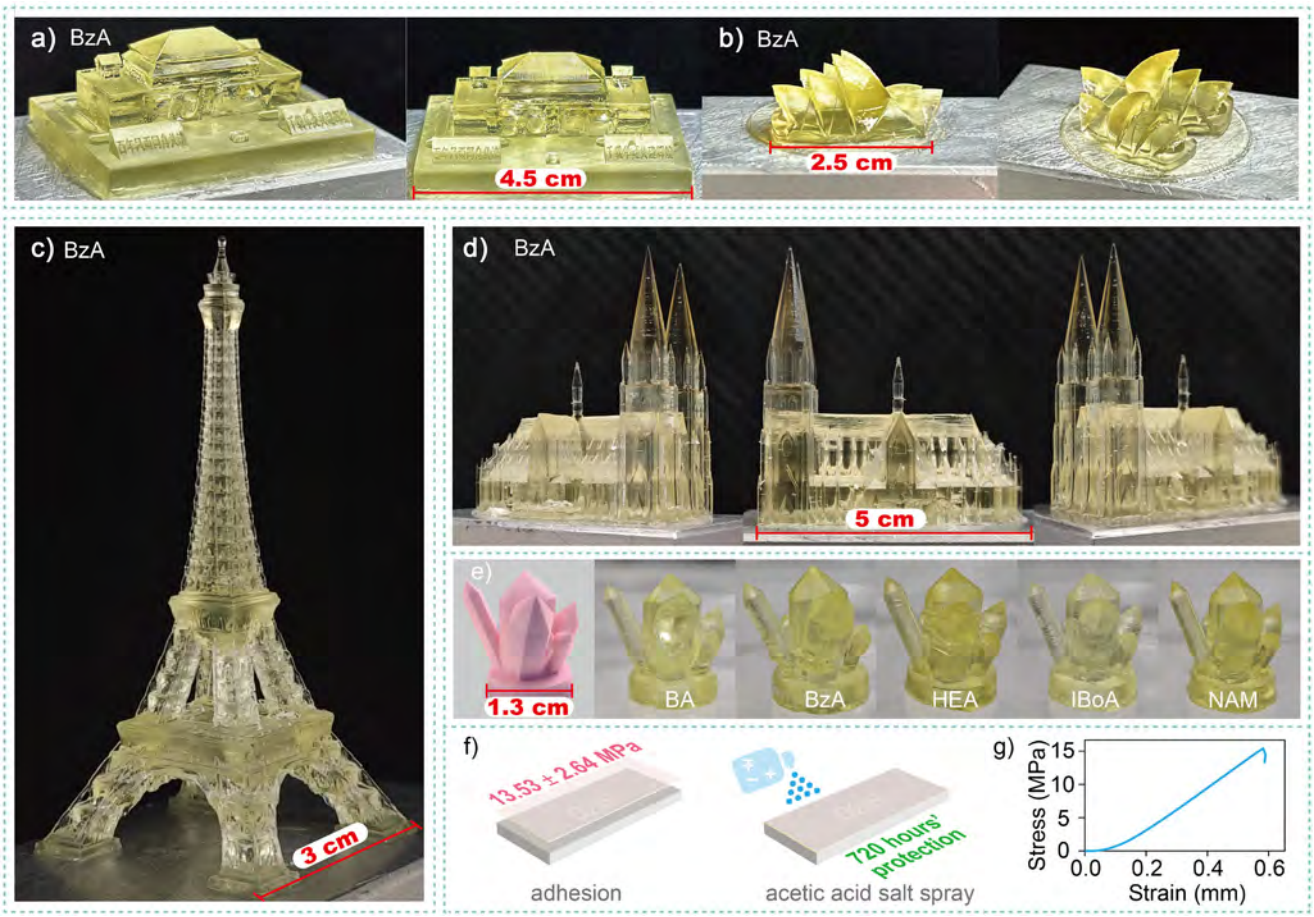

Figure 3. a–d) 3D-printed world landmark replicas fabricated using the BzA-based resin. e) Models printed using different resins. f) Schematic illustration of the anticorrosion coating strategy based on DTI-mediated photoiniferter polymerization, highlighting coating adhesion and salt spray resistance performance on Q235 steel. g) Stress–strain curve from the pull-out test of the photo-cured coating.

squared deviation (RMSD) between the printed object and the digital model, yielding an RMSD of 0.10–0.22 mm which however does not represent the vertical or lateral feature resolution alone, and the minimum feature size was determined to be 0.25 mm (see more details in Section S11.1).

Advanced Anticorrosion Coating

We also validated the technology's layer-based efficacy by using it to apply an anticorrosion coating to Q235 steel (Figure 3i). An IBoA-based resin with a BDDA crosslinker was formulated for this purpose. The resulting photo-cured coating demonstrated adhesion strength of 13.53 ± 2.64 MPa (Section S12.1), which is higher than that of a photo-initiated system (1.42 ± 2.56 MPa; Section S12.1). The coated steel sample was then subjected to an acetic acid salt spray test (AASS) for 720 h (30 days; Section S12.2). The coating showed no signs of corrosion or deterioration, offering exceptional protection. We hypothesize that this superior performance is due to the homogeneous polymer network created by the controlled polymerization, which minimizes defects and distributes stress evenly, thus providing a more effective barrier against corrosion.

Conclusion

Employing a computer-guided strategy based on structure–property–performance relationships, we have designed a new photoiniferter, DTI. Computational analyses predicted that DTI would offer enhanced polymerization kinetics, control, and oxygen tolerance compared to the benchmark DTP, which was confirmed experimentally. DTI achieved a (k_p^{app} of 0.809 min^{-1} for MA polymerization, which is over four times faster than DTP ($k_p^{app} = 0.196$ min^{-1}) under equivalent conditions, while maintaining polymerization control ($Đ < 1.1$). DTI also demonstrated better oxygen tolerance, retaining 65.9% of its k_p^{app} under air-purging at 1 mL 30 s^{-1} compared to only 13.3% for DTP. This performance enabled DLP 3D printing with rapid layer curing times of 8 s using low-viscosity resins, and the fabrication of anticorrosion coatings with an adhesion strength of 13.53 MPa and 720 h resistance to acetic acid salt spray.

Acknowledgements

C.W. thanks the Taishan Scholar Foundation of Shandong Province (No. tsqn202312054) and the National Natural Science Foundation of China (Grant No. 22101155). C.B. thanks Australian Research Council for his Australian Laureate Fellowship (FL220100016).

Conflict of Interests

The authors declare no conflict of interest.

Data Availability Statement

The data that support the findings of this study are available in the supplementary material of this article.

Keywords: 3D printing · Photo-controlled polymerization · Photoiniferter · RAFT · Reversible deactivation

[1] N. Shahrubudin, T. C. Lee, R. Ramlan, *Procedia Manuf.* **2019**, *35*, 1286–1296.
[2] C. Sun, N. Fang, D. M. Wu, X. Zhang, *Sens. Actuators A Phys.* **2005**, *121*, 113–120.
[3] X. Zheng, J. Deotte, M. P. Alonso, G. R. Farquar, T. H. Weisgraber, S. Gemberling, H. Lee, N. Fang, C. M. Spadaccini, *Rev. Sci. Instrum.* **2012**, *83*, 125001.
[4] S. C. Gauci, A. Vranic, E. Blasco, S. Bräse, M. Wegener, C. Barner-Kowollik, *Adv. Mater.* **2024**, *36*, 2306468.
[5] Y. Yagci, S. Jockusch, N. J. Turro, *Macromolecules* **2010**, *43*, 6245–6260.
[6] F. Di Lorenzo, S. Seiffert, *Polym. Chem.* **2015**, *6*, 5515–5528.
[7] A. P. Dhand, M. D. Davidson, H. M. Zlotnick, T. J. Kolibaba, J. P. Killgore, J. A. Burdick, *Science* **2024**, *385*, 566–572.
[8] M. Si, M. Zhou, W. Zhang, G. Shi, Y. He, X. Qiao, W. Fan, X. Pang, *Polym. Chem.* **2024**, *15*, 3121–3126.
[9] Y. Xiu, V. A. Bobrin, N. Corrigan, J. Zhang, C. Boyer, *Macromol. Rapid Commun.* **2023**, *44*, 2300236.
[10] Y. B. Cakir, H. C. Kiliclar, Y. Yagci, *React. Funct. Polym.* **2023**, *191*, 105656.
[11] E. Goldbach, X. Allonas, C. Croutxé-Barghorn, C. Ley, L. Halbardier, G. L'Hostis, *Eur. Polym. J.* **2023**, *188*, 111947.
[12] C. Wu, N. Corrigan, C.-H. Lim, W. Liu, G. Miyake, C. Boyer, *Chem. Rev.* **2022**, *122*, 5476–5518.
[13] N. D. Dolinski, Z. A. Page, E. H. Discekici, D. Meis, I. H. Lee, G. R. Jones, R. Whitfield, X. Pan, B. G. McCarthy, S. Shanmugam, et al., *J. Polym. Sci. A Polym. Chem.* **2019**, *57*, 268–273.
[14] B. P. Fors, C. J. Hawker, *Angew. Chem. Int. Ed.* **2012**, *51*, 8850–8853.
[15] N. J. Treat, H. Sprafke, J. W. Kramer, P. G. Clark, B. E. Barton, J. Read de Alaniz, B. P. Fors, C. J. Hawker, *J. Am. Chem. Soc.* **2014**, *136*, 16096–16101.
[16] S. Allison-Logan, Q. Fu, Y. Sun, M. Liu, J. Xie, J. Tang, G. G. Qiao, *Angew. Chem. Int. Ed.* **2020**, *59*, 21392–21396.
[17] K. Matyjaszewski, J. Xia, *Chem. Rev.* **2001**, *101*, 2921–2990.
[18] C. Boyer, V. Bulmus, T. P. Davis, V. Ladmiral, J. Liu, S. Perrier, *Chem. Rev.* **2009**, *109*, 5402–5436.
[19] G. Moad, E. Rizzardo, S. H. Thang, *Chem. Asian J.* **2013**, *8*, 1634–1644.
[20] M. Chen, M. Zhong, J. A. Johnson, *Chem. Rev.* **2016**, *116*, 10167–10211.
[21] D. A. Corbin, G. M. Miyake, *Chem. Rev.* **2021**, *122*, 1830–1874.
[22] G. Moad, E. Rizzardo, S. H. Thang, *Polymer* **2008**, *49*, 1079–1131.
[23] G. Moad, E. Rizzardo, S. H. Thang, *Aust. J. Chem.* **2005**, *58*, 379–410.
[24] M. L. Coote, *Macromolecules* **2004**, *37*, 5023–5031.
[25] M. L. Coote, E. H. Krenske, E. I. Izgorodina, *Macromol. Rapid Commun.* **2006**, *27*, 473–497.
[26] M. L. Coote, L. Radom, *J. Am. Chem. Soc.* **2003**, *125*, 1490–1491.
[27] D. Matioszek, S. Mazières, O. Brusylovets, C. Y. Lin, M. L. Coote, M. Destarac, S. Harrisson, *Macromolecules* **2019**, *52*, 3376–3386.
[28] Z. Zhang, N. Corrigan, A. Bagheri, J. Jin, C. Boyer, *Angew. Chem. Int. Ed.* **2019**, *58*, 17954–17963.
[29] V. A. Bobrin, J. Zhang, N. Corrigan, C. Boyer, *Adv. Mater. Technol.* **2023**, *8*, 2201054.

[30] X. Shi, J. Zhang, N. Corrigan, C. Boyer, *Mater. Chem. Front.* **2021**, *5*, 2271–2282.
[31] C. W. A. Bainbridge, A. Wangsadijaya, N. Broderick, J. Jin, *Polym. Chem.* **2022**, *13*, 1484–1494.
[32] Z. Zhang, N. Corrigan, C. Boyer, *Angew. Chem. Int. Ed.* **2022**, *61*, e202114111.
[33] X. Shi, J. Zhang, N. Corrigan, C. Boyer, *Polym. Chem.* **2022**, *13*, 44–57.
[34] B. Zhao, J. Li, Y. Xiu, X. Pan, Z. Zhang, J. Zhu, *Macromolecules* **2022**, *55*, 1620–1628.
[35] B. Zhao, J. Li, Z. Li, X. Lin, X. Pan, Z. Zhang, J. Zhu, *Macromolecules* **2022**, *55*, 7181–7192.
[36] K. Lee, N. Corrigan, C. Boyer, *Angew. Chem. Int. Ed.* **2021**, *60*, 8839–8850.
[37] H. J. B. Chua, A. A. Rosser, C. M. Fellows, T. C. Brown, A. Bagheri, *ACS Appl. Polym. Mater.* **2024**, *6*, 10853–10864.
[38] L. Qiao, M. Zhou, G. Shi, Z. Cui, X. Zhang, P. Fu, M. Liu, X. Qiao, Y. He, X. Pang, *J. Am. Chem. Soc.* **2022**, *144*, 9817–9826.
[39] B. Huang, Y. Zhou, L. Wei, R. Hu, X. Zhang, P. Coates, F. Sefat, W. Zhang, C. Lu, *Ind. Eng. Chem. Res.* **2022**, *61*, 13052–13062.
[40] A. Bagheri, C. M. Fellows, C. Boyer, *Adv. Sci.* **2021**, *8*, 2003701.
[41] H. Quan, T. Zhang, H. Xu, S. Luo, J. Nie, X. Zhu, *Bioact. Mater.* **2020**, *5*, 110–115.
[42] F. Chen, R. Li, J. Sun, G. Lu, J. Wang, B. Wu, J. Li, J. Nie, X. Zhu, *J. Appl. Polym. Sci.* **2021**, *138*, 49965.
[43] J. Tu, K. Makarian, N. J. Alvarez, G. R. Palmese, *Materials* **2020**, *13*, 4109.
[44] Z. Wang, C. Wu, W. Liu, *Polymers* **2024**, *16*, 323.
[45] R. W. Hughes, M. E. Lott, R. A. Olson S, B. S. Sumerlin, *Prog. Polym. Sci.* **2024**, *156*, 101871.
[46] M. Hartlieb, *Macromol. Rapid Commun.* **2022**, *43*, 2100514.
[47] T. Otsu, *J. Polym. Sci. A Polym. Chem.* **2000**, *38*, 2121–2136.
[48] J. Xu, S. Shanmugam, N. A. Corrigan, C. Boyer, in *Controlled Radical Polymerization: Mechanisms*, American Chemical Society, Washington, DC **2015**, pp. 247–267.
[49] J. I. Bowman, C. B. Eades, M. A. Vratsanos, N. C. Gianneschi, B. S. Sumerlin, *Angew. Chem. Int. Ed.* **2023**, *62*, e202309951.
[50] Z. Wu, Z. He, Y. Zhou, T. Kou, K. Gong, F. Nan, T. T. Bezuneh, S. Han, C. Boyer, W. W. Yu, *Angew. Chem. Int. Ed.* **2025**, *64*, e202422975.
[51] A.-C. Lehnen, J. Gurke, A. M. Bapolisi, M. Reifarth, M. Bekir, M. Hartlieb, *Chem. Sci.* **2023**, *14*, 593–603.
[52] A.-C. Lehnen, J. A. M. Kurki, M. Hartlieb, *Polym. Chem.* **2022**, *13*, 1537–1546.
[53] R. W. Hughes, M. E. Lott, J. I. Bowman, B. S. Sumerlin, *ACS Macro Lett.* **2023**, *12*, 14–19.
[54] M. L. Coote, L. Radom, *Macromolecules* **2004**, *37*, 590–596.
[55] A. R. S. Santha Kumar, S. Allison-Logan, J. R. Finnegan, N. K. Singha, M. Ashokkumar, G. Qiao, *ACS Macro Lett.* **2023**, *12*, 1012–1018.
[56] R. A. L. Wylie, V. F. Jafari, G. G. Qiao, *Macromolecules* **2024**, *57*, 3731–3740.
[57] L. Camdžic, E. E. Stache, *Macromolecules* **2024**, *57*, 9250–9256.
[58] M. A. Beres, J. Y. Rho, A. Kerr, T. Smith, S. Perrier, *Polym. Chem.* **2024**, *15*, 522–533.
[59] J. Lee, Y. Kwon, C. Yu, D. Konkolewicz, M. S. Kwon, *Polym. Chem.* **2025**, *16*, 1798–1806.
[60] A. J. Wong, C. B. Eades, J. I. Bowman, C. L. G. Davidson, B. S. Sumerlin, *Polym. Chem.* **2025**, *16*, 620–625.
[61] E. K. Stacy, M. L. McCormick, K. C. Stevens, P. E. Jankoski, J. Aguinaga, D. L. Patton, B. S. Sumerlin, T. D. Clemons, *ACS Macro Lett.* **2024**, *13*, 1662–1669.
[62] Y. Xia, G. M. Scheutz, C. P. Easterling, J. Zhao, B. S. Sumerlin, *Angew. Chem. Int. Ed.* **2021**, *60*, 18537–18541.
[63] P. J. Hurst, J. Yoon, R. Singh, M. F. Abouchaleh, K. A. Stewart, B. S. Sumerlin, J. P. Patterson, *Macromol. Rapid Commun.* **2024**, *45*, 2400100.
[64] M. E. Lott, L. Trachsel, E. Schué, C. L. G. I. V. Davidson, R. A. Olson S, D. I. Pedro, F. Chang, Y. Hong, W. G. Sawyer, B. S. Sumerlin, *Macromolecules* **2024**, *57*, 4007–4015.
[65] M.-N. Antonopoulou, N. P. Truong, T. Egger, A. A. Kroeger, M. L. Coote, A. Anastasaki, *Angew. Chem. Int. Ed.* **2025**, *64*, e202420733.
[66] G. Irvine, K. Myronidis, F. Pinto, M. Kope, *Angew. Chem. Int. Ed.* **2025**, *64*, e202421970.
[67] R. A. Olson, M. E. Lott, J. B. Garrison, C. L. Davidson IV, L. Trachsel, D. I. Pedro, W. G. Sawyer, B. S. Sumerlin, *Macromolecules* **2022**, *55*, 8451–8460.
[68] M. L. Allegrezza, N. D. A. Watuthanthrige, Y. Wang, G. A. Garcia, H. Ren, D. Konkolewicz, *Polym. Chem.* **2020**, *11*, 6129–6133.
[69] M. L. Allegrezza, Z. M. DeMartini, A. J. Kloster, Z. A. Digby, D. Konkolewicz, *Polym. Chem.* **2016**, *7*, 6626–6636.
[70] C. Barner-Kowollik, M. Buback, B. Charleux, M. L. Coote, M. Drache, T. Fukuda, A. Goto, B. Klumperman, A. B. Lowe, J. B. Mcleary, *J. Polym. Sci. A Polym. Chem.* **2006**, *44*, 5809–5831.
[71] Q. Ma, G. G. Qiao, Z. An, *Angew. Chem. Int. Ed.* **2023**, *62*, e202314729.
[72] M. Zhang, S. P. Armes, Z. An, *Macromolecules* **2025**, *58*, 507–515.
[73] M. Zhang, S. P. Armes, Z. An, *ACS Macro Lett.* **2025**, *14*, 306–312.
[74] J. Li, X. Pan, N. Li, J. Zhu, X. Zhu, *Polym. Chem.* **2018**, *9*, 2897–2904.
[75] S. Lian, P. Armes Steven, Z. An, *CCS Chem.* **2024**, *7*, 2304–2314.
[76] S. Zhu, W. Kong, S. Lian, A. Shen, S. P. Armes, Z. An, *Nat. Synth.* **2025**, *4*, 15–30.
[77] J. Li, C. Wu, Y. Lei, W. Liu, *J. Phys. Chem. Lett.* **2022**, *13*, 3290–3296.
[78] F. Neese, F. Wennmohs, U. Becker, C. Riplinger, *J. Chem. Phys.* **2020**, *152*, 224108.
[79] J.-D. Chai, M. Head-Gordon, *J. Chem. Phys.* **2008**, *128*, 084106.
[80] S. Grimme, J. Antony, S. Ehrlich, H. Krieg, *J. Chem. Phys.* **2010**, *132*, 154104.
[81] F. Weigend, R. Ahlrichs, *Phys. Chem. Chem. Phys.* **2005**, *7*, 3297–3305.
[82] A. V. Marenich, C. J. Cramer, D. G. Truhlar, *J. Phys. Chem. B* **2009**, *113*, 6378–6396.
[83] T. Lu, F. Chen, *J. Comput. Chem.* **2012**, *33*, 580–592.
[84] W. Humphrey, A. Dalke, K. Schulten, *J. Mol. Graph.* **1996**, *14*, 33–38.
[85] L. V. Lutkus, S. S. Rickenbach, T. M. McCormick, *J. Photochem. Photobiol. A* **2019**, *378*, 131–135.
[86] I. M. Irshadeen, S. L. Walden, M. Wegener, V. X. Truong, H. Frisch, J. P. Blinco, C. Barner-Kowollik, *Journal of the American Chemical Society* **2021**, *143*, 21113–21126.
[87] F. Pashley-Johnson, X. Wu, J. A. Carroll, S. L. Walden, H. Frisch, A.-N. Unterreiner, F. E. Du Prez, H.-A. Wagenknecht, J. Read de Alaniz, B. L. Feringa, et al., *Angew. Chem. Int. Ed.* **2025**, *64*, e202502651.
[88] S. L. Walden, J. A. Carroll, A.-N. Unterreiner, C. Barner-Kowollik, *Adv. Sci.* **2024**, *11*, 2306014, accessed: 2025-10-07.
[89] S. Shanmugam, J. Xu, C. Boyer, *J. Am. Chem. Soc.* **2015**, *137*, 9174–9185.
[90] M. N. Gupta, R. Batra, R. Tyagi, A. Sharma, *Biotechnol. Prog.* **1997**, *13*, 284–288.
[91] J. Xu, K. Jung, A. Atme, S. Shanmugam, C. Boyer, *J. Am. Chem. Soc.* **2014**, *136*, 5508–5519.

Manuscript received: September 06, 2025
Revised manuscript received: November 11, 2025
Manuscript accepted: November 11, 2025
Version of record online: ■■, ■■